nature chemistry

ARTICLES

https://doi.org/10.1038/s41557-019-0304-z

Identifying the components of the solid–electrolyte interphase in Li-ion batteries

Luning Wang[1], Anjali Menakath[2], Fudong Han[3], Yi Wang[1], Peter Y. Zavalij[1], Karen J. Gaskell[1], Oleg Borodin[4], Dinu Iuga[2], Steven P. Brown[2], Chunsheng Wang[1,3*], Kang Xu[4*] and Bryan W. Eichhorn[1*]

The importance of the solid–electrolyte interphase (SEI) for reversible operation of Li-ion batteries has been well established, but the understanding of its chemistry remains incomplete. The current consensus on the identity of the major organic SEI component is that it consists of lithium ethylene di-carbonate (LEDC), which is thought to have high Li-ion conductivity, but low electronic conductivity (to protect the Li/C electrode). Here, we report on the synthesis and structural and spectroscopic characterizations of authentic LEDC and lithium ethylene mono-carbonate (LEMC). Direct comparisons of the SEI grown on graphite anodes suggest that LEMC, instead of LEDC, is likely to be the major SEI component. Single-crystal X-ray diffraction studies on LEMC and lithium methyl carbonate (LMC) reveal unusual layered structures and Li^+ coordination environments. LEMC has Li^+ conductivities of $>1\times10^{-6}$ S cm^{-1}, while LEDC is almost an ionic insulator. The complex interconversions and equilibria of LMC, LEMC and LEDC in dimethyl sulfoxide solutions are also investigated.

Li-ion batteries (LIBs) are ubiquitous in twenty-first-century life and have an estimated 2018 global market amounting to US$ 25 billion. Despite their technological importance and mass production, a molecular-level understanding of the ion transport mechanisms and interfacial chemistry in these devices remains elusive. As evidenced by the history of LIBs[1], misconceptions about the fundamental chemistry have often delayed breakthroughs in new materials—indeed, interphases on graphite anodes are a conspicuous example. Graphitic materials serve as the standard anodes in current LIBs. In the charge and discharge processes of a LIB, Li^+ intercalates into and de-intercalates from the graphene layers[2–7]. Due to the extremely low potentials where such intercalation/de-intercalation processes occur (~0.2 V versus Li^+/Li)[4,8,9], commonly used carbonate-based electrolytes (for example 1 M $LiPF_6$ in ethylene carbonate (EC)/dimethyl carbonate (DMC)) are electrochemically reduced at the anode surface in the first few charge/discharge cycles[9–11]. This electrochemical reduction generates an insoluble passivating film on the anode surface known as the solid–electrolyte interphase (SEI)[12–16], which is a critical component of LIBs in that it prevents further parasitic electrolyte decomposition and stabilizes battery operation and capacity[7,12,13]. The SEI is still regarded as one of the most important but least understood components in rechargeable LIBs, although extensive efforts have been devoted to elucidating its composition and function[17]. It is well accepted that the SEI is ~10–50 nm thick[7,14,18–23], contains inorganic salts (for example, Li_2CO_3 and LiF)[14,18,20,24,25] with degraded carbonate molecules (semi-carbonates and polymers)[10,15,24,26–32] and prevents further solvent degradation as an electronic insulator while facilitating Li^+ transport as an electrolyte[7,12,13]. However, the precise structure, composition and functional mechanism(s) of the SEI remain under debate.

It is well accepted that the organic SEI component primarily arises from the electrochemical reduction of EC, as is often indicated by a narrow shoulder in the discharge curve at ~0.8 V during the first discharge cycle (Fig. 1)[13,33,34]. The importance of EC-originated products in the SEI is evidenced by the necessity of employing EC in essentially all commercial electrolytes, where preferential solvation of Li^+ by EC dictates SEI formation[35,36]. EC reduction is commonly believed to react via a 'single-electron pathway' that generates lithium ethylene di-carbonate (LEDC) according to equation (1)[10,15,26,28,37]. Identification of LEDC in authentic nanoscopic SEI films has been accomplished through multiple spectroscopic techniques including X-ray photoelectron spectroscopy (XPS)[10,14,33], Fourier-transform infrared spectroscopy (FTIR)[10,15,26,28,31,33,38], solid-state and solution-phase NMR spectroscopy[14,32,39,40], to name a few. The SEI spectroscopic signatures were compared to those of synthetic LEDC standards, which have been independently reported by four separate laboratories, including one of us[37,39,41,42]. Unfortunately, these synthetic procedures for LEDC synthesis suffer from insolubility problems that lead to kinetic limitations in the carbonate formation process. Here, we report that these reported synthetic standards are not LEDC but are actually lithium ethylene mono-carbonate (LEMC). To our knowledge LEDC has not been prepared prior to our work.

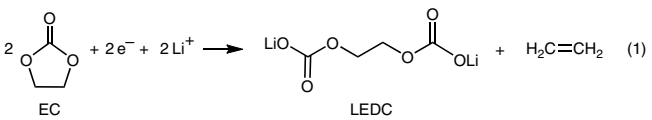

Here, we describe high-yield synthetic routes to LEDC·2DMSO, LEMC and lithium methyl carbonate (LMC). These compounds have been fully characterized using FTIR, 1D and 2D solution and solid-state NMR spectroscopy (^{1}H, ^{13}C and ^{7}Li), as well as powder X-ray diffraction (XRD) for all compounds and single-crystal X-ray studies for LEMC and LMC. In addition, we also show that LEMC

[1]Department of Chemistry and Biochemistry, University of Maryland, College Park, MD, USA. [2]Department of Physics, University of Warwick, Coventry, UK. [3]Department of Chemical and Biomolecular Engineering, University of Maryland, College Park, MD, USA. [4]Electrochemistry Branch, Power and Energy Division Sensor and Electron Devices Directorate, US Army Research Laboratory, Adelphi, MD, USA. *e-mail: cswang@umd.edu; conrad.k.xu.civ@mail.mil; eichhorn@umd.edu

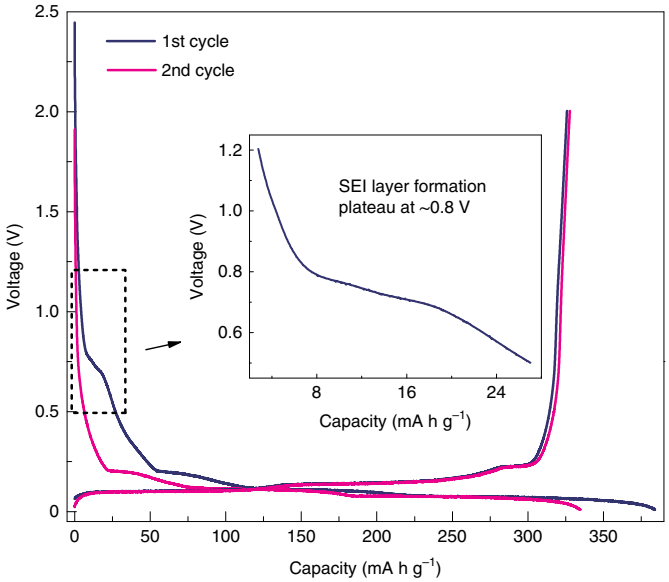

Fig. 1 | Electrochemical behaviour of a graphite electrode. The first (blue) and second (pink) battery cycles, respectively, with 1 M $LiPF_6$ in EC/DMC (vol:vol = 1:1) as electrolyte solution and Li foil as the counter electrode. Inset, the formation of SEI layers at a plateau of ~0.8 V in the first lithiation process of the graphite electrode.

is a facile Li^+ ion conductor, whereas LEDC and LMC are not. Spectroscopic comparisons between authentic EC/DMC-derived SEI films and the synthetic model compounds suggest that the SEI probably contains an LMC-capped LEMC organic layer and it is unlikely that LEDC is present in the SEI at all.

Results and discussion

Synthesis and characterization. LEMC was conveniently prepared in high yield as a white polycrystalline solid through the lithiation/deprotonation of ethylene glycol (EG) with *n*-BuLi according to Fig. 2a. Single crystals of LEMC were obtained from EG solutions layered with pyridine in ~10% yield. LMC was prepared in high yield in a similar manner, according to published procedures (Fig. 2b)[37,39,41]. Single crystals of LMC were grown from a MeOH/Et_2O solution in ~30% yield. Synthetic details for both compounds are provided in the Methods and Supplementary Information along with full spectroscopic, analytical and structural data (FTIR, solution and solid-state NMR, elemental analysis, powder and single-crystal XRD, XPS; Supplementary Figs. 1–10 and Supplementary Tables 1–5). These white crystalline solids are soluble in rigorously dried DMSO but insoluble in ethereal and hydrocarbon solvents. LEMC is also soluble in dry EG, moderately moisture sensitive and will slowly decompose in air. LMC is soluble in MeOH and dimethylformamide, is air/moisture-sensitive and also undergoes hydrolysis in solution.

Previous reports on the synthesis of LEDC involved nucleophilic addition of di-lithium ethylene glycolate ($LiOCH_2CH_2OLi$) to CO_2 in ethereal solvents[37,39,41]. The reaction of EG with excess lithiation agents (*n*-BuLi or LiH) was expected to yield the di-lithium ethylene glycolate intermediate, which subsequently reacts with CO_2 in ethereal solutions. However, it appears that the mono-lithiated intermediate, $LiOCH_2CH_2OH$ (LiEG), is virtually insoluble in ethereal solvents and precipitates from solution before the second deprotonation can occur. We have found that addition of excess CO_2(g) to the heterogeneous mixture results in an initial deactivation of the excess *n*-BuLi, followed by a slower carbonate formation reaction with sparingly soluble $LiOCH_2CH_2OH$ to give LEMC

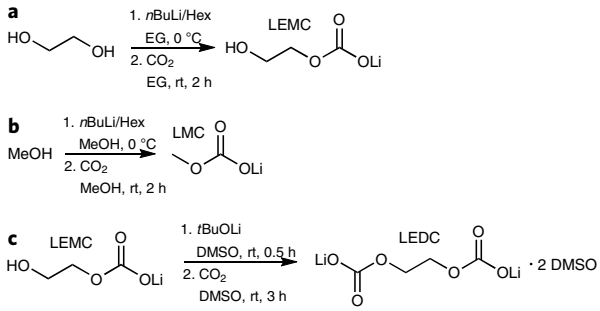

Fig. 2 | Preparation of LEMC, LMC and LEDC. a–c, Chemical synthesis of LEMC (**a**), LMC (**b**) and LEDC·2DMSO (**c**).

as the exclusive product. The experimental and calculated powder XRD and FTIR data for the analytically pure LEMC single crystals from our studies are perfect matches to all previously reported data for LEDC, indicating that these studies actually characterized LEMC (Supplementary Figs. 11 and 12). With this knowledge, we employed the more convenient synthesis of LEMC involving direct deprotonation of EG with *n*-BuLi at 0 °C, as described in Fig. 2a.

On recognizing the solubility issues associated with the lithium glycolate intermediates, we devised an alternative synthesis of LEDC from LEMC in DMSO solutions. White polycrystalline LEDC·2DMSO was conveniently prepared through the deprotonation of LEMC by lithium *tert*-butoxide in DMSO, followed by reaction with excess CO_2 (Fig. 2c). The powder precipitates from solution in high yield and is slightly soluble in rigorously dry DMSO. The solid and its solutions are sensitive to moisture and other protic sources and are also air-sensitive. Spectroscopic and analytical data (FTIR, solution and solid-state NMR, elemental analysis; Supplementary Figs. 5–8) reveal a composition of $LiOCO_2CH_2CH_2OCO_2Li{\cdot}2(OSMe_2)$ or LEDC·2DMSO. So far, we have been unable to isolate single crystals of the compound, and the precipitates give broad powder XRD profiles (Supplementary Fig. 1). Regardless, the analytical and spectroscopic data, specifically the NMR data (see below), unequivocally show that the compound is LEDC·2DMSO. Removal of DMSO solvates from the crystalline lattice of LEDC·2DMSO was accomplished by sonication in anhydrous THF at 50 °C, which generated amorphous LEDC, as indicated by powder XRD and NMR studies (Supplementary Figs. 1 and 13).

Crystal structures of LEMC and LMC. The solid-state structures of LMC and LEMC were determined from single-crystal X-ray studies of the respective crystals. Details of the refinements and crystallographic data are provided in the Supplementary Information (crystallographic file and Supplementary Tables 2 and 3). LMC is monoclinic, space group $P2_1/c$, and contains two independent LMC molecules in the asymmetric unit that are partitioned into two different layers of the crystal lattice (Fig. 3a,b). Layer A contains double sheets of LMC molecules with LiO_4 tetrahedra at the layer interior and the Me groups on the layer exterior. Each oxygen of the LiO_4 tetrahedra originates from a terminal carbonate oxygen of a different LMC molecule, three from one side and one from the other side of the layer, which links the structure into a two-dimensional (2D) network via edge-shared tetrahedra. Although layer A is perfectly ordered, layer B has a 3:2 positional disorder in the *y*–*z* plane but is otherwise identical to A. The two layers alternately stack along the *x* axis of the cell to give an unusual order–disorder–order layered structure of functionally identical subunits. The LiO_4 tetrahedra are somewhat distorted with Li–O bond distances that vary from 1.922(6) to 2.011(6) Å (average of 1.960(2) Å) and O–Li–O angles that vary from 88.9(3)° to 117.2(3)°.

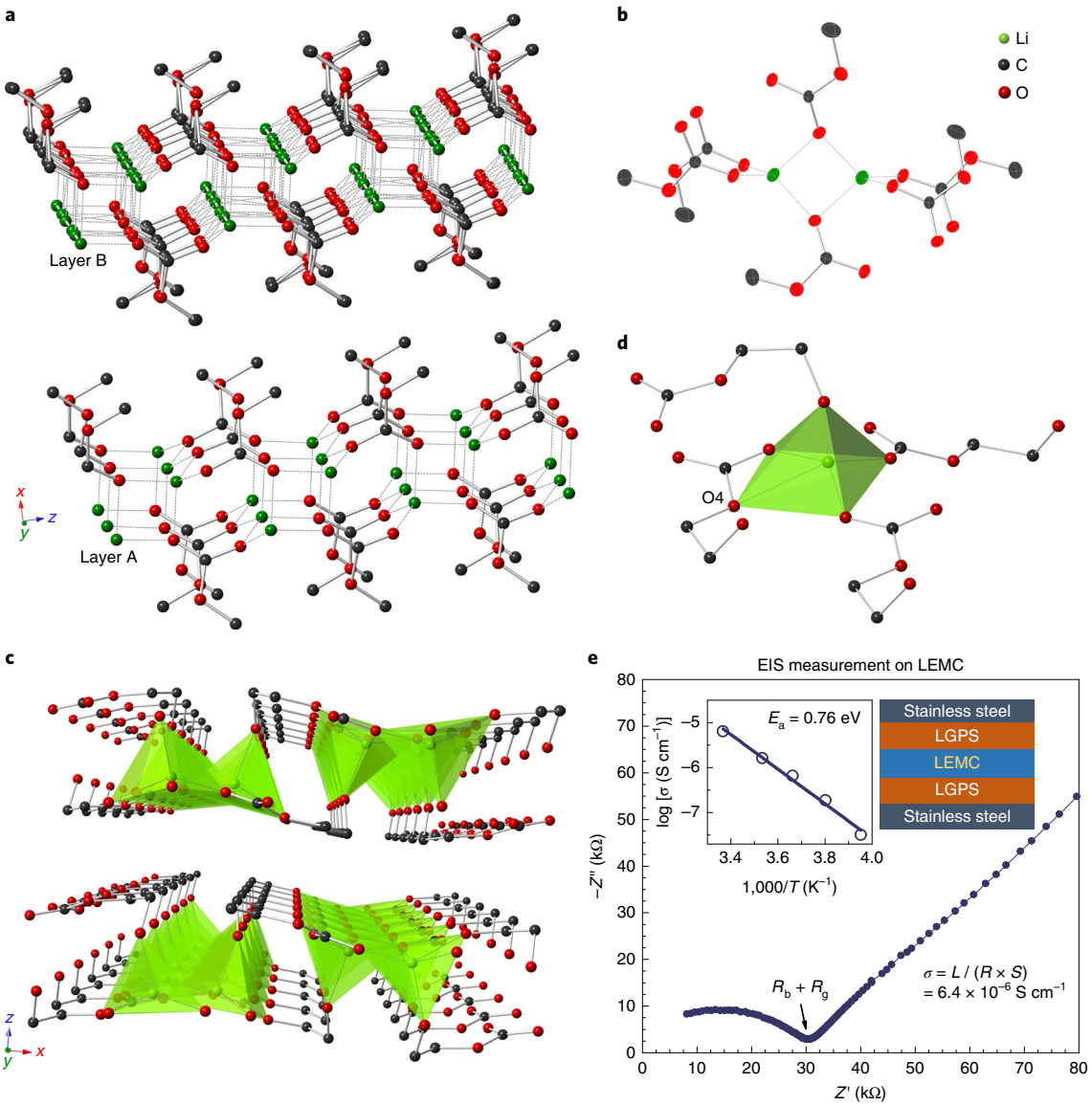

Fig. 3 | X-ray structures of LMC and LEMC, and EIS measurements on LEMC. a,**b**, Structures of LMC showing the alternative packing of ordered layer A and disordered layer B (**a**) and the tetrahedral coordination of Li^+ by O atoms (**b**). **c**,**d**, Structures of LEMC showing the layers of LEMC double sheets (**c**) and the distorted pentagonal pyramidal five-coordinate Li^+ ion polyhedron (**d**). **e**, The ionic conductivity of LEMC measured by EIS at 25 °C. Inset (left), linear fit used to calculate the activation energy (E_a) for Li^+ conductivity. The scheme (right inset) shows the electrochemical cell used for EIS measurements, where the LEMC layer is sandwiched between LGPS layers to block proton transfer. Ionic conductivity σ was calculated from the thickness L of the LEMC film, the resistance measured by EIS ($R = R_b + R_g$) and the area S of LEMC in the cell.

LEMC is orthorhombic, space group *Pbcn*, and contains a single unique molecule in the asymmetric unit. The structure contains double sheets of LEMC molecules stacked along the z axis of the orthorhombic cell (Fig. 3c,d), but the Li^+ ions are in distorted five-coordinate pentagonal prismatic environments defined by three terminal carbonate oxygens, one alkyl carbonate oxygen and an alcohol oxygen. Four of the Li–O bonds are typical (1.917(8)–2.027(9) Å; average of 1.996(4) Å) with a longer 2.580(9) Å contact to the alkyl carbonate oxygen O4. The pentagonal prisms share corners to form double ribbons running in the y direction that are linked together in the x direction by the spanning alcohol groups of the LEMC. Unlike the LMC structure, the Li^+ ions in LEMC reside in Li–O–Li–O lined crevices on the exterior of the layers. This unusual Li^+ coordination geometry and its position in the interlayer crevices of the layered lattice structure may play an important role in the Li^+-ion conductivity described in the next section.

Li-ion conductivities. As both LMC and LEMC (reported as LEDC in prior publications) have frequently been reported as key organic components of the SEI on graphite electrodes, information about their Li^+ ion conductivities are of great importance and are measured here by electrochemical impedance spectroscopy (EIS). Cold-pressed LEMC pellets are sandwiched between two $Li_{10}GeP_2S_{12}$ (LGPS)[43,44] rectifiers to block any proton conductivity during measurements (see Methods for details). The EIS data and the Arrhenius plot for the Li^+ conductivity of LEMC are shown in Fig. 3e. LEMC has a reasonably high Li-ion conductivity of 6.4×10^{-6} S cm^{-1} at 25 °C, which is slightly better than that of single-domain LiPON films ($\sigma \approx 3 \times 10^{-6}$ S cm^{-1})[45]. The activation energy (E_a) for Li^+ conductivity calculated from an Arrhenius analysis is 0.76 eV (Fig. 3e, inset and Supplementary Fig. 14), which is higher than for common inorganic Li^+ conductors but similar to organic-based Li^+ ion conductors, such as $LiClO_4$/poly(ethylene oxide)[43,45,46]. The influences

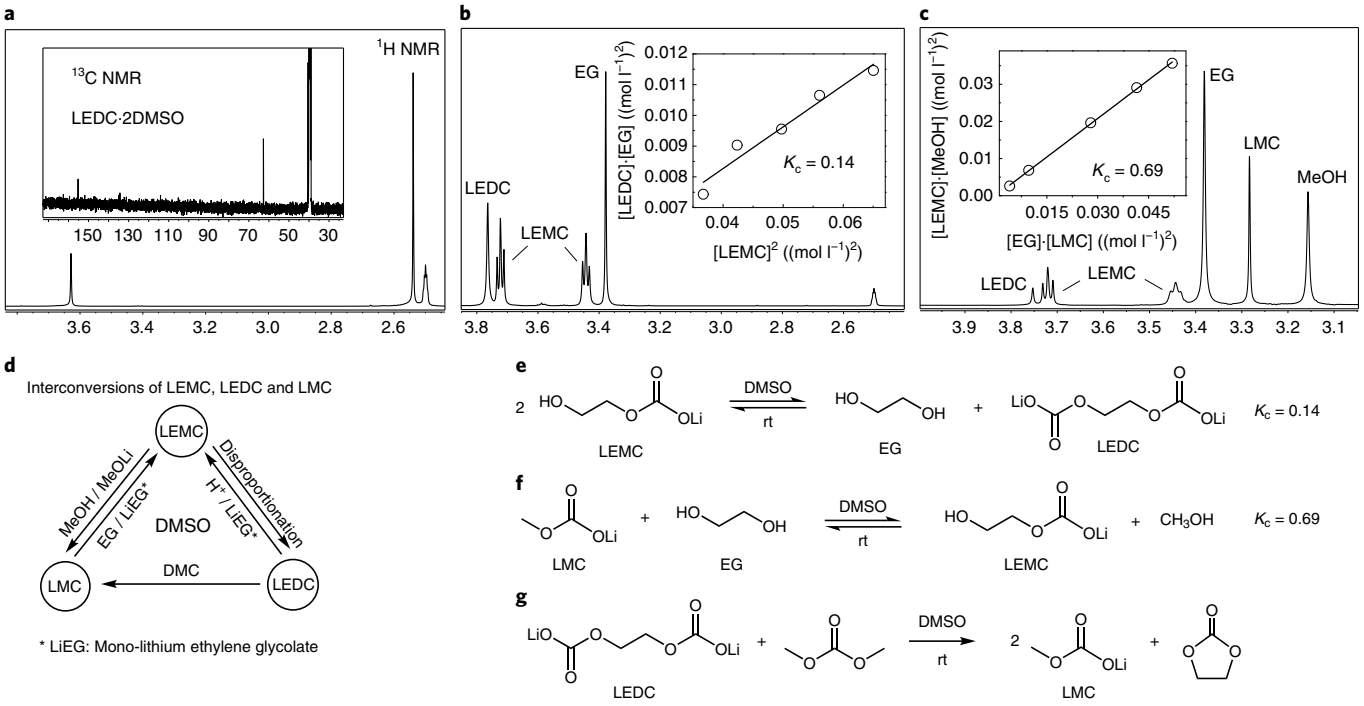

Fig. 4 | Solution NMR studies on LMC, LEMC and LEDC·2DMSO. a–c, NMR spectra (500 MHz, 25 °C) of LEDC·2DMSO (saturated, ~0.02 mol l^{-1}) (**a**), LEMC (initial concentration, 0.53 mol l^{-1}) (**b**) and LMC + EG (initial concentration, LMC 0.34 mol l^{-1} + EG 0.41 mol l^{-1}) (**c**). The NMR spectra were collected in DMSO-d_6 and indicate complex equilibria. Inset in **a** shows ^{13}C NMR spectrum of LEDC·2DMSO, while insets in **b** and **c** show linear fittings used to calculate the equilibrium constants. **d–g**, Interconversions between these lithium organic carbonates, in reactions with alcohols and carbonate electrolytes in DMSO.

of OH rotation, Li^+ interstitials and Li^+ and H^+ vacancies on Li^+ diffusion in LEMC were examined using Born–Oppenheimer molecular dynamics (BOMD) simulations of the superheated LEMC (Supplementary Figs. 15 and 16). Addition of Li^+ vacancies or Li^+ substitution for H in the O–H groups results in the fastest Li^+ diffusion, followed by Li^+ interstitial diffusion occurring via a 'knock-off' mechanism[23] that is similar to Li_2CO_3, where the five-fold Li–O coordination environment significantly decreases the Li^+ diffusion barriers[23]. Measurements on the amorphous LEDC and LMC (pressed pellets) give resistances outside the measurable range, which we attribute to high resistivities ($<1\times10^{-9}$ S cm^{-1}) of the two compounds. The high resistivity measured for LMC is consistent with previous studies[47].

Solution properties and NMR studies. In contrast to previous reports[41,48], our studies show that LEMC and LMC, as well as LEDC·2DMSO, dissolve to give stable solutions in rigorously dry DMSO. However, all three compounds undergo aggregation in the solution that leads to concentration-dependent chemical shifts in the ^{1}H, ^{13}C and ^{7}Li NMR spectra. Moreover, the compounds are reactive towards water, residual solvent (MeOH, EG, EC or DMC) and are involved in complex equilibria and interconversions. Details of the solution chemistry and the spectroscopic properties are provided in Fig. 4 and Supplementary Figs. 17–20, and will be described in a subsequent publication. Only the pertinent properties are presented here.

Solution ^{1}H and ^{13}C {^{1}H} NMR spectra for LEDC·2DMSO in DMSO-d_6 are shown in Fig. 4a and Supplementary Fig. 5. Solid-state 1D ^{1}H and ^{7}Li magic-angle spinning (MAS) NMR spectra, along with 2D ^{1}H (SQ)-^{1}H (DQ) and ^{7}Li-^{1}H MAS NMR spectra are provided in Supplementary Figs. 6 and 7. The 1D solid-state NMR spectra of LMC and LEMC simulated using the density functional theory gauge-including projector-augmented wave (GIPAW) approach[49,50] demonstrate high consistency with experimental data (Supplementary Fig. 6 and Supplementary Tables 4 and 5). In DMSO-d_6 solution (saturated solution, ~20 mmol l^{-1}, 25 °C), the LEDC ethylene protons give rise to a singlet at 3.63 ppm with the ethylene and carbonate carbons appearing at 62.7 and 155.2 ppm, respectively, which is consistent with the symmetry of the compound. In the solid state, ^{1}H NMR resonances appear at 3.4 and 2.6 ppm, which are assigned to the ethylene protons and lattice DMSO, respectively.

On account of its lower symmetry, the ethylene protons of LEMC appear as two triplets at 3.44 and 3.72 ppm with an *OH* resonance at 4.82 ppm (DMSO-d_6, initial concentration 0.53 mol l^{-1}, 25 °C), with similar shifts in the solid state (Supplementary Fig. 6). The ethylene carbons and the carbonate carbon appear at 61.0, 65.8 and 156.9 ppm, respectively. However, LEMC quickly establishes an equilibrium with LEDC and EG in solution ($K_c = 0.14$), as illustrated in Fig. 4b,e. Adding EG or LEDC to the solutions shift the equilibria to the left, as expected. Similarly, adding EG to a pure solution of LEDC·2DMSO will generate LEMC according to the equilibrium expression (Supplementary Fig. 18). These data not only establish that LEMC readily reaches equilibria in solution but also confirm the identity of LEDC through the equilibrium relationship.

The alkyl carbonates are quite reactive towards protic solvents such as water, alcohols and the carbonate solvents EC and DMC. For example, hydrolysis of LEDC gives rise to LEMC, in both DMSO-d_6 solutions and the solid state (monitored by NMR and FTIR spectroscopies, respectively; Supplementary Figs. 21 and 22). LEMC and LMC show much higher stability towards moisture than LEDC, but all three compounds will be hydrolysed eventually to give corresponding alcoholic species (FTIR and simulation studies, Supplementary Figs. 23–25). In addition, the alkyl carbonates can

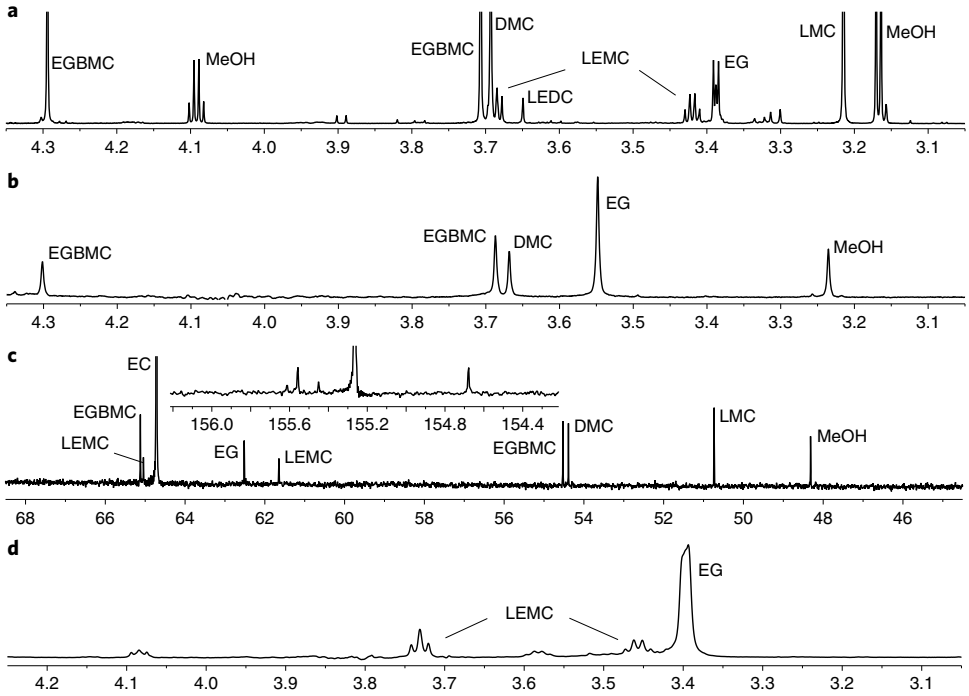

Fig. 5 | Solution NMR characterizations of the graphite SEI layer. a–d, Spectra collected from SEIs generated in electrolyte solutions of 1 M $LiPF_6$ in EC/DMC: ^{1}H NMR, DMSO-d_6 (**a**), ^{1}H NMR, 0.1 M DCl in D_2O (**b**) and ^{13}C {^{1}H} NMR, DMSO-d_6 (**c**). **d**, ^{1}H NMR spectra in DMSO-d_6 of SEI layers generated in the electrolyte solution of $LiPF_6$/EC. NMR spectra in **a**,**c** and **b**,**d** were collected at 25 °C with an 800 MHz and 500 MHz spectrometer, respectively.

be interconverted in DMSO solutions through the addition of complementary carbonates or alcohols. The interconversions of LMC and LEMC through the addition of EG and MeOH are illustrated in Fig. 4c,f ($K_c = 0.69$), while the conversion of LEDC to LMC through reaction with DMC is presented in Fig. 4g (for NMR spectra see Supplementary Fig. 17). Dissolving LEMC and DMC together in DMSO-d_6 instantly results in multiple equilibria (Fig. 4e–g) and products such as EG, LMC, LEDC and MeOH (Supplementary Fig. 20). An overview of the interconversion chemistries that occur with LMC, LEMC and LEDC is provided in Fig. 4d (for supporting spectra see Supplementary Fig. 17). The interconversions only occur in DMSO solutions (as DMSO solvates the species) and do not occur (or only occur slowly at the liquid–solid interface) when insoluble LEDC, LEMC or LMC are in contact with pure EC/DMC solvents in a battery environment. Analysis of the reactions where LEDC or LEMC is suspended in DMC or EC/DMC solutions (without DMSO) is presented in Supplementary Fig. 26.

Chemical compositions of SEI layers on graphite electrodes. Because SEI layers are only 10–50 nm thick, isolating enough material to evaluate by traditional spectroscopic methods (for example, NMR) is a challenge. To overcome this problem, we fabricated large and thoroughly dried electrodes containing at least 400 mg graphite (TIMREX KS44) coated on Cu current collectors (~200 cm^2). The electrodes were cycled three times from 0.7 to 2.0 V versus Li/Li$^+$ to generate SEI layers. Three types of electrolyte, 1 M $LiPF_6$ in EC/DMC (vol:vol = 1:1), 1 M $LiPF_6$ in DMC and 1 M $LiPF_6$ in EC, were used (mixing 1.52 g $LiPF_6$ and 13 g EC forms a liquid solution at 27 °C). The electrochemical performances of the three systems are shown in Supplementary Fig. 27. When EC is included in the electrolyte solutions, a plateau at ~0.8 V is observed in the first cycle but disappears in subsequent ones, indicating the formation of SEI layers. However, when only DMC is used, no such plateau is observed. These data are consistent with literature studies indicating that SEI layers are formed in the first discharge cycle and originate from EC. Previous works have demonstrated continuous evolution of SEI layers during battery cycling[21,22], but we only focus on the initial step in SEI formation here (the 0.8 V plateau in the first discharge process).

The SEI films were extracted into both DMSO-d_6 and 0.1 M DCl in D_2O for solution NMR analysis. Representative 1D and 2D spectra are given in Fig. 5 and Supplementary Figs. 28 and 29. Both the aqueous and DMSO extracts show significant quantities of ethylene glycol bis(methyl carbonate) (EGBMC) originating from catalytic reactions of EC/DMC with oxides (for example, a surface oxide layer on the Cu current collector or methoxide), which is well documented in the literature[38,51]. The 0.1 M DCl extraction method instantly hydrolyses possible SEI candidates (for example, LEMC, LMC and LEDC) to give methanol and EG (Fig. 5b). Control experiments (Supplementary Figs. 30 and 31) show that the complex equilibria and secondary chemical reactions described above are averted and the observed EG:MeOH ratio provides an accurate measure of the ratio of EC-derived SEI products (for example, LEMC + LEDC) to DMC-derived SEI products (for example, LMC) present in the SEI film. The DMSO-d_6 extracts of SEI layers formed in 1 M $LiPF_6$/EC/DMC electrolytes contain LEMC, LEDC, EG, LMC and MeOH, as well as residual EC and DMC. The NMR spectra in Fig. 5d collected on SEI layers grown in the EC-only cell, where DMC, as well as DMC-related equilibria/interconversions are excluded, indicate the presence of LEMC. Solid-state ^{1}H MAS NMR characterizations of the SEI layers coated on graphite powders, unfortunately, give very broad peaks, possibly due to the presence of paramagnetic impurities in the electrodes (Supplementary Fig. 32).

The equilibrated DMSO-d_6 SEI extracts show that the primary SEI candidates (LEMC, LEDC and LMC) are indeed present, but the complex equilibria and secondary reactions described above prohibit the determination of their origin (that is, were they present in the SEI). The hydrolysed SEI extracts suggest that the ratio between EC-derived SEI products (for example, LEMC and LEDC)

and DMC-derived SEI products (for example, LMC) is ~5:1 in all the repeated measurements. However, electrodes cycled in 1 M $LiPF_6$ in pure DMC result in no LMC formation and no 0.8 V SEI plateau in the first discharge cycle. These findings suggest that a significant LMC component is present in SEI films but that it results from a secondary chemical reaction with LEMC or LEDC. Control experiments of insoluble LEMC powders suspended in pure DMC (and EC/DMC mixture) for several weeks indicate a slow surface reaction at the solid–liquid interface that transforms LEMC into LMC and MeOH (equation (2) and Supplementary Fig. 26): However, the suspended powders are primarily LEMC after several weeks at room temperature, suggesting that the particles contain a core of LEMC surrounded by a thin shell of LMC. Similar chemical transformations occur with LEDC as well (Supplementary Fig. 26).

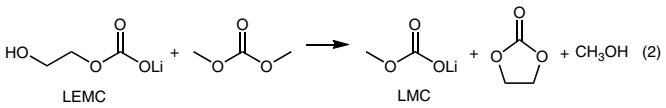

(2)

While we cannot unequivocally determine whether LEDC or LEMC (or both) are the initial and primary components of the SEI, our hypothesis is that LEMC is the major SEI constituent and LEDC does not exist (or does not persist) in the typical LIB environment. This proposal is based on the following observations: (1) a number of previous studies have linked the organic SEI component to the LEDC standard[28,39,41], which was actually LEMC, (2) LEDC is highly reactive towards residual protons, which are ubiquitous in all cell assemblies, from trace moisture in bulk electrolytes to surface functionalities on graphite. The presence of EG (or LiEG) in the EC-only control cell (which was rigorously dried) is a direct measure of the protio impurities in battery components. The protio impurities would probably convert any LEDC into LEMC. Thus, even if LEDC were formed through the single-electron reduction pathway (equation (1)), it is probably converted to LEMC and LMC through reactions with protons and DMC, respectively, due to its inability to 'survive' in the LIB environment.

Formation and evolution of LEMC on graphite electrode. Although LEMC is probably a key component in the graphite SEIs, the precise mechanism of its formation remains unclear. It is possible that LEDC is generated as the first step[10,15], but a subsequent hydrolysis/protonation transforms it to LEMC, as suggested by our model chemical and computational studies (Supplementary Figs. 21 and 22). In addition, we have discovered two alternative pathways for LEMC formation involving nucleophilic addition of OH^- (Supplementary Fig. 33) and MeO^- to EC (Supplementary Fig. 34). LiOH is a well-known component of the inorganic SEI layer[7,24] and can be converted to LEMC in a heterogeneous transformation. LiOMe is known to exist in DMC-derived SEIs[7,24,27] and its participation in electrolyte degradation through nucleophilic reactions has been thoroughly investigated[51].

The evolution of the SEI layer with battery cycling is well known[21,22] and reactions of LEMC are probably part of that process. For example, the heterogeneous reaction of LEMC with DMC (equation (2)) forms an LMC-capped LEMC organic layer, which should self-terminate in a dense layered structure (that is, DMC cannot access the LEMC beneath the LMC surface). We believe that LEMC persists in a well-functioning SEI and facilitates Li^+ ion transfer. The well-established need for EC as the indispensable component in carbonate-based electrolytes[6,52] strongly implicates an active EC-derived compound in an effective SEI, which we attribute to LEMC. The relatively high Li^+ conductivity of LEMC probably benefits SEI function, in contrast to LMC, which is a bulk insulator. The alcoholic proton (R-OH) on LEMC may well be subject to electrochemical reduction, generating partially di-lithiated ethylene mono-carbonate (DLEMC) and H_2 (equation (3)): Our computational studies suggest that DLEMC has equivalent or better Li^+ ion conductivity than LEMC (Supplementary Section 1.7). However, we always detect a significant fraction of the protonated LEMC in the electrode analyses.

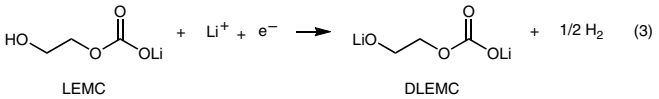

(3)

In conclusion, we have demonstrated, through rigorous and comprehensive characterizations including single-crystal and powder XRD, FTIR, elemental analysis, solid-state and liquid 1D and 2D NMR spectroscopy, that the previously synthesized chemical standard, LEDC, is actually LEMC. NMR studies on the SEI layers grown on graphite electrodes in typical LIBs with 1 M $LiPF_6$ in EC/DMC electrolyte indicate that it is highly likely that LEMC, instead of LEDC, prevails as the major organic component in the SEI layers. These lithium organic carbonates, including LMC, LEMC and LEDC, show complex interconversions/equilibria in DMSO solutions. In a battery environment, these compounds (LEMC and LMC) appear to be formed through secondary chemical reactions and are not generated through direct electrochemical reduction. The identification of LEMC and its properties (ionic conductivity, chemical reactivity) provide insight into Li^+ ion transport across SEIs and pave the way for future engineering of artificial interphases with superior properties.

Methods

General. Details on chemical syntheses, chemical/electrochemical characterizations and SEI extractions are provided in the Supplementary Information.

Synthesis of LMC. All the synthetic procedures were carried out under inert atmospheres unless otherwise stated. To a Schlenk flask of magnetically stirred anhydrous methanol (20 ml) at 0 °C was added 2.5 M *n*-BuLi/hexane (10 ml, 25 mmol) dropwise. The reaction was warmed to room temperature and further stirred for 30 min. Afterwards, CO_2 gas dried over a $CaSO_4$ column was bubbled through the solution for 2 h at room temperature. The solvents were removed in vacuo, leaving a white powder that was further rinsed with anhydrous diethyl ether. The resulting white powder was dried under vacuum for 12 h to afford LMC (1.8 g, 88% yield). Large needle crystals suitable for single-crystal XRD studies were obtained from a methanol/diethyl ether solvent mixture.

Synthesis of LEMC. To a Schlenk flask of magnetically stirred anhydrous EG (20 ml) at 0 °C was added 1.6 M MeLi/diethyl ether (25 ml, 40 mmol) or 2.5 M *n*-BuLi/hexane (16 ml, 40 mmol), dropwise. The reaction was warmed to room temperature and stirred for 30 min. The diethyl ether (or hexane) was removed in vacuo, leaving a suspension of LiEG in EG. Dry CO_2 was bubbled through the suspension for 2 h under fast stirring, whereby the solid precipitates gradually dissolved and a clear but viscous solution was obtained. Afterwards, anhydrous pyridine (50 ml) was added to the solution. The EG/pyridine solution was stored at room temperature for 2 days under an inert atmosphere, during which time copious amounts of white powder precipitated from solution. The precipitates were collected through centrifugation, rinsed with anhydrous DMF and anhydrous diethyl ether, and further dried under vacuum for 12 h to afford LEMC (1.6 g, 36% yield). Large crystals suitable for single-crystal X-ray studies were obtained from the solvent mixture of EG/pyridine.

Synthesis of LEDC·2DMSO. To a Schlenk flask charged with a stirred solution of LEMC (224 mg, 2.0 mmol) dissolved in anhydrous DMSO (20 ml) was added lithium *tert*-butoxide (240 mg, 3.0 mmol, 1.5 equiv.) at room temperature. All powders dissolved and the clear solution was stirred for 30 min. Dry CO_2 was bubbled through the stirred solution for 3 h, during which time a white powder precipitated from solution. The white powder was collected by centrifugation, rinsed with anhydrous diethyl ether and dried in vacuo for 12 h to afford white microcrystalline LEDC·2DMSO (440 mg, 68% yield).

EIS measurements. To preclude contributions from the hydroxyl protons in LEMC that may contribute to the total ionic conductivities, we measured the impedance of analytically pure LEMC pressed pellets sandwiched between two LGPS rectifiers. LGPS has very high Li^+ ionic conductivity ($>10^{-2}$ S cm^{-1}) but does not transport protons[43,44] and, as such, all measured transport is due to Li^+-ion conduction. A proton-blocking cell, stainless steel/LGPS/LEMC/LGPS/stainless steel, was assembled to measure the Li ion conductivity of LEMC. The cell was prepared by cold-pressing 20 mg LGPS, 140 mg LEMC and 20 mg LGPS powders

together under 360 MPa for 3 min. The EIS spectrum of the cell was measured from 1 MHz to 0.1 Hz using an electrochemical workstation (Solartron 1287/1260). The intercept with the Z' axis is attributed to the resistance (R) from the bulk electrolyte and grain boundaries. The ionic conductivity (σ) is determined by L/RS, where L and S are the thickness and area of the electrolyte, respectively. The ionic conductivity of LMC and LEDC was also measured with the same method but without LGPS as proton-blocking medium.

Data availability

Crystallographic data for the structures reported in this work have been deposited at the Cambridge Crystallographic Data Centre (CCDC) under deposition nos. CCDC 1847784 (LEMC) and CCDC 1847785 (LMC). Copies of the data can be obtained free of charge via www.ccdc.cam.ac.uk/structures. Data supporting the findings of this study are available within this paper and its Supplementary Information, and are available from the corresponding author upon reasonable request. The MAS NMR experimental and GIPAW calculated data for this study are provided as a supporting dataset from WRAP, the Warwick Research Archive Portal at http://wrap.warwick.ac.uk/120226.

Received: 15 October 2018; Accepted: 26 June 2019;
Published online: 19 August 2019

References

1. Winter, M., Barnett, B. & Xu, K. Before Li ion batteries. *Chem. Rev.* **118**, 11433–11456 (2018).
2. Yazami, R. & Touzain, P. A reversible graphite-lithium negative electrode for electrochemical generators. *J. Power Sources* **9**, 365–371 (1983).
3. Persson, K. et al. Lithium diffusion in graphitic carbon. *J. Phys. Chem. Lett.* **1**, 1176–1180 (2010).
4. Persson, K., Hinuma, Y., Meng, Y. S., Van der Ven, A. & Ceder, G. Thermodynamic and kinetic properties of the Li-graphite system from first-principles calculations. *Phys. Rev. B* **82**, 125416 (2010).
5. Goodenough, J. B. & Kim, Y. Challenges for rechargeable Li batteries. *Chem. Mater.* **22**, 587–603 (2010).
6. Xu, K. Electrolytes and interphases in Li-ion batteries and beyond. *Chem. Rev.* **114**, 11503–11618 (2014).
7. Verma, P., Maire, P. & Novák, P. A review of the features and analyses of the solid electrolyte interphase in Li-ion batteries. *Electrochim. Acta* **55**, 6332–6341 (2010).
8. Dahn, J. R., Zheng, T., Liu, Y. & Xue, J. Mechanisms for lithium insertion in carbonaceous materials. *Science* **270**, 590 (1995).
9. Levi, M. D. & Aurbach, D. The mechanism of lithium intercalation in graphite film electrodes in aprotic media. Part 1. High resolution slow scan rate cyclic voltammetric studies and modeling. *J. Electroanal. Chem.* **421**, 79–88 (1997).
10. Aurbach, D., Markovsky, B., Shechter, A., Ein-Eli, Y. & Cohen, H. A comparative study of synthetic graphite and Li electrodes in electrolyte solutions based on ethylene carbonate-dimethyl carbonate mixtures. *J. Electrochem. Soc.* **143**, 3809–3820 (1996).
11. Zhang, X., Kostecki, R., Richardson, T. J., Pugh, J. K. & Ross, P. N. Electrochemical and infrared studies of the reduction of organic carbonates. *J. Electrochem. Soc.* **148**, A1341–A1345 (2001).
12. Peled, E. The electrochemical behavior of alkali and alkaline earth metals in nonaqueous battery systems—the solid electrolyte interphase model. *J. Electrochem. Soc.* **126**, 2047–2051 (1979).
13. Fong, R., Von Sacken, U. & Dahn, J. R. Studies of lithium intercalation into carbons using nonaqueous electrochemical cells. *J. Electrochem. Soc.* **137**, 2009–2013 (1990).
14. Nie, M. et al. Lithium ion battery graphite solid electrolyte interphase revealed by microscopy and spectroscopy. *J. Phys. Chem. C* **117**, 1257–1267 (2013).
15. Aurbach, D. et al. The study of electrolyte solutions based on ethylene and diethyl carbonates for rechargeable Li batteries II. Graphite electrodes. *J. Electrochem. Soc.* **142**, 2882–2890 (1995).
16. Winter, M., Novák, P. & Monnier, A. Graphites for lithium-ion cells: the correlation of the first-cycle charge loss with the Brunauer–Emmett–Teller surface area. *J. Electrochem. Soc.* **145**, 428–436 (1998).
17. Winter, M. The solid electrolyte interphase—the most important and the least understood solid electrolyte in rechargeable Li batteries. *Z. Phys. Chem.* **223**, 1395–1406 (2009).
18. Edström, K., Herstedt, M. & Abraham, D. P. A new look at the solid electrolyte interphase on graphite anodes in Li-ion batteries. *J. Power Sources* **153**, 380–384 (2006).
19. Yoshida, T. et al. Degradation mechanism and life prediction of lithium-ion batteries. *J. Electrochem. Soc.* **153**, A576–A582 (2006).
20. Malmgren, S. et al. Comparing anode and cathode electrode/electrolyte interface composition and morphology using soft and hard X-ray photoelectron spectroscopy. *Electrochim. Acta* **97**, 23–32 (2013).
21. Lu, P., Li, C., Schneider, E. W. & Harris, S. J. Chemistry, impedance and morphology evolution in solid electrolyte interphase films during formation in lithium ion batteries. *J. Phys. Chem. C* **118**, 896–903 (2014).
22. Zhuo, Z. et al. Breathing and oscillating growth of solid–electrolyte-interphase upon electrochemical cycling. *Chem. Commun.* **54**, 814–817 (2018).
23. Shi, S. et al. Direct calculation of Li-ion transport in the solid electrolyte interphase. *J. Am. Chem. Soc.* **134**, 15476–15487 (2012).
24. Zhuang, G. V. & Ross, P. N. Analysis of the chemical composition of the passive film on Li-ion battery anodes using attentuated total reflection infrared spectroscopy. *Electrochem. Solid State Lett.* **6**, A136–A139 (2003).
25. Meyer, B. M., Leifer, N., Sakamoto, S., Greenbaum, S. G. & Grey, C. P. High field multinuclear NMR investigation of the SEI layer in lithium rechargeable batteries. *Electrochem. Solid State Lett.* **8**, A145–A148 (2005).
26. Aurbach, D. & Gofer, Y. The behavior of lithium electrodes in mixtures of alkyl carbonates and ethers. *J. Electrochem. Soc.* **138**, 3529–3536 (1991).
27. Augustsson, A. et al. Solid electrolyte interphase on graphite Li-ion battery anodes studied by soft X-ray spectroscopy. *Phys. Chem. Chem. Phys.* **6**, 4185–4189 (2004).
28. Zhuang, G. V., Xu, K., Yang, H., Jow, T. R. & Ross, P. N. Lithium ethylene dicarbonate identified as the primary product of chemical and electrochemical reduction of EC in 1.2 M $LiPF_6$/EC: EMC electrolyte. *J. Phys. Chem. B* **109**, 17567–17573 (2005).
29. Zhuang, G. V., Yang, H., Blizanac, B. & Ross, P. N. A study of electrochemical reduction of ethylene and propylene carbonate electrolytes on graphite using ATR-FTIR spectroscopy. *Electrochem. Solid State Lett.* **8**, A441–A445 (2005).
30. Shkrob, I. A., Zhu, Y., Marin, T. W. & Abraham, D. Reduction of carbonate electrolytes and the formation of solid-electrolyte interface (SEI) in lithium-ion batteries. 2. Radiolytically induced polymerization of ethylene carbonate. *J. Phys. Chem. C* **117**, 19270–19279 (2013).
31. Tsubouchi, S. et al. Spectroscopic characterization of surface films formed on edge plane graphite in ethylene carbonate-based electrolytes containing film-forming additives. *J. Electrochem. Soc.* **159**, A1786–A1790 (2012).
32. Ota, H., Sakata, Y., Wang, X., Sasahara, J. & Yasukawa, E. Characterization of lithium electrode in lithium imides/ethylene carbonate and cyclic ether electrolytes II. Surface chemistry. *J. Electrochem. Soc.* **151**, A437–A446 (2004).
33. Kang, S.-H., Abraham, D., Xiao, A. & Lucht, B. Investigating the solid electrolyte interphase using binder-free graphite electrodes. *J. Power Sources* **175**, 526–532 (2008).
34. Liu, P. & Wu, H. Construction and destruction of passivating layer on Li_xC_6 in organic electrolytes: an impedance study. *J. Power Sources* **56**, 81–85 (1995).
35. Xu, K. & von Wald Cresce, A. Li^+-solvation/desolvation dictates interphasial processes on graphitic anode in Li ion cells. *J. Mater. Res.* **27**, 2327–2341 (2012).
36. von Wald Cresce, A., Borodin, O. & Xu, K. Correlating Li^+ solvation sheath structure with interphasial chemistry on graphite. *J. Phys. Chem. C* **116**, 26111–26117 (2012).
37. Aurbach, D., Daroux, M., Faguy, P. & Yeager, E. Identification of surface films formed on lithium in propylene carbonate solutions. *J. Electrochem. Soc.* **134**, 1611–1620 (1987).
38. Shi, F. et al. A catalytic path for electrolyte reduction in lithium-ion cells revealed by in situ attenuated total reflection–Fourier transform infrared spectroscopy. *J. Am. Chem. Soc.* **137**, 3181–3184 (2015).
39. Gireaud, L., Grugeon, S., Laruelle, S., Pilard, S. & Tarascon, J.-M. Identification of Li battery electrolyte degradation products through direct synthesis and characterization of alkyl carbonate salts. *J. Electrochem. Soc.* **152**, A850–A857 (2005).
40. Michan, A. L., Leskes, M. & Grey, C. P. Voltage dependent solid electrolyte interphase formation in silicon electrodes: monitoring the formation of organic decomposition products. *Chem. Mater.* **28**, 385–398 (2015).
41. Xu, K. et al. Syntheses and characterization of lithium alkyl mono-and dicarbonates as components of surface films in Li-ion batteries. *J. Phys. Chem. B* **110**, 7708–7719 (2006).
42. Seo, D. M. et al. Reduction reactions of carbonate solvents for lithium ion batteries. *ECS Electrochem. Lett.* **3**, A91–A93 (2014).
43. Kamaya, N. et al. A lithium superionic conductor. *Nat. Mater.* **10**, 682 (2011).
44. Han, F., Gao, T., Zhu, Y., Gaskell, K. J. & Wang, C. A battery made from a single material. *Adv. Mater.* **27**, 3473–3483 (2015).
45. Knauth, P. Inorganic solid Li ion conductors: an overview. *Solid State Ion.* **180**, 911–916 (2009).
46. Gurusiddappa, J., Madhuri, W., Suvarna, R. P. & Dasan, K. P. Studies on the morphology and conductivity of PEO/$LiClO_4$. *Mater. Today Proc.* **3**, 1451–1459 (2016).
47. Schafzahl, L. et al. Long-chain Li and Na alkyl carbonates as solid electrolyte interphase components: structure, ion transport and mechanical properties. *Chem. Mater.* **30**, 3338–3345 (2018).
48. Zhuang, G. V., Yang, H., Ross, P. N., Xu, K. & Jow, T. R. Lithium methyl carbonate as a reaction product of metallic lithium and dimethyl carbonate. *Electrochem. Solid State Lett.* **9**, A64–A68 (2006).

49. Pickard, C. J. & Mauri, F. All-electron magnetic response with pseudopotentials: NMR chemical shifts. *Phys. Rev. B* **63**, 245101 (2001).
50. Yates, J. R., Pickard, C. J. & Mauri, F. Calculation of NMR chemical shifts for extended systems using ultrasoft pseudopotentials. *Phys. Rev. B* **76**, 024401 (2007).
51. Gachot, G. et al. Deciphering the multi-step degradation mechanisms of carbonate-based electrolyte in Li batteries. *J. Power Sources* **178**, 409–421 (2008).
52. Xu, K. Whether EC and PC differ in interphasial chemistry on graphitic anode and how. *J. Electrochem. Soc.* **156**, A751–A755 (2009).

Acknowledgements

The authors thank the DOE for funding this research through the EFRC (NEES-II) and Energy Hub (JCESR). B.W.E. thanks J. Davis for many helpful discussions. A.M. thanks the University of Warwick for a Chancellor's International Scholarship. The UK 850 MHz solid-state NMR Facility used in this research is funded by EPSRC and BBSRC, as well as the University of Warwick, including via part funding through Birmingham Science City Advanced Materials Projects 1 and 2 supported by Advantage West Midlands (AWM) and the European Regional Development Fund (ERDF). O.B. acknowledges support via NASA agreement NND16AA29I.

Author contributions

B.W.E., K.X. and C.W. designed and conceived the study. L.W. directed the project and contributed chemical synthesis, battery/electrode tests, FTIR and solution NMR studies. F.H. and C.W. performed ionic conductivity experiments and analysis. A.M., S.P.B. and D.I. contributed solid-state NMR measurements and analysis. P.Y.Z. and Y.W. contributed single-crystal growth and crystallographic studies. K.G. performed XPS experiments and analysis. O.B. conducted quantum chemistry calculations. B.W.E. supervised the project. All authors contributed to discussions and preparation of the manuscript.

Competing interests

The authors declare no competing interests.

Additional information

Supplementary information is available for this paper at https://doi.org/10.1038/s41557-019-0304-z.

Reprints and permissions information is available at www.nature.com/reprints.

Correspondence and requests for materials should be addressed to C.W., K.X. or B.W.E.

Publisher's note: Springer Nature remains neutral with regard to jurisdictional claims in published maps and institutional affiliations.